Magnetization Dynamics of Single and Trilayer Permalloy Nanodots

Mahathi Kuchibhotla[1], Abhishek Talapatra[2] Arabinda Haldar[1*] and Adekunle Olusola Adeyeye[2,3]

[1]Department of Physics, Indian Institute of Technology Hyderabad, Kandi 502284, Telangana, India

[2]*Information Storage Materials Laboratory, Department of Electrical and Computer Engineering, National University of Singapore, Singapore 117576*

[3]Department of Physics, Durham University, South Road, Durham, DH1 3LE, United Kingdom

*Corresponding authors: Electronic address: arabinda@phy.iith.ac.in

Abstract

We have investigated the magnetization dynamics in single and trilayer circular Permalloy nanodots of diameter 120 nm using broadband ferromagnetic resonance spectroscopy. For the single layer nanodots, two well-separated modes near the saturation field; a high-frequency center mode due to the excitations at the center of the nanodots and a low-frequency edge mode due to the inhomogeneous effective field near the edges were observed. Both the center mode and the edge mode are found to be sensitive to the thickness of the nanodots. However, for the trilayer nanodots, two center modes arise due to the in-phase and out-of-phase precession of spins in magneto-dynamically coupled layers. Our experimental results are substantiated by micromagnetic simulations, which are in good agreement.

Keywords: Ferromagnetic resonance, Magnetic multilayer nanodots, Magnetic vortex, Spin dynamics, Deep UV lithography, Micromagnetic simulation

Introduction

Magnetization dynamics in patterned nanostructures are important in spintronics based device applications. Laterally confined nanostructures like quantum-dot, magnetic nanowires, nanodots have emerging applications in magnetic logic,[1,2] high-density data storage[3] and microwave signal processing devices.[4,5] Such devices offer non-volatility, low power consumption, high-speed operation and high-density data storage. Thus, spintronics is a promising alternative to the current semiconductor-based complementary metal oxide semiconductor (CMOS) technology. Among different geometrically confined nanostructures, magnetically soft circular nanodots have attained considerable attention due to the presence of vortex configuration at ground state with negligible coercivity and it exhibits rich spin dynamic spectra. These nanodots are found to have potential applications in magnetic random access memory,[6] vortex-based transistors,[7] spin-torque nano-oscillators,[8] magnetic logic and sensors.[9]

The ground state of soft magnetic nanodots with an appropriate aspect ratio (the dot thickness to radius ratio) shows a vortex state which has in-plane curling and perpendicular magnetization at the core due to the competition between exchange and dipolar interactions.[10,11] At remanence, there are low-frequency (sub-GHz) modes corresponding to the gyrotropic motion of vortex core and high-frequency (> 1 GHz) radial and azimuthal modes of the vortex.[12–14] With the application of the magnetic field, vortex and saturated magnetic states are observed at low and high field regions respectively.[15] With the increase in the aspect ratio, the effective field becomes inhomogeneous near the edges. This leads to the edge mode (EM) in addition to the center or fundamental FMR (Ferromagnetic resonance) mode observed in nanodot. The edge mode is noticed when the spin precession is localized near the edges of the nanodot. This particularly arises due to the inhomogeneous demagnetizing field near the edges. However, the fundamental or center

mode (CM) is characterized by the maximum amplitude of spin precession at the center of the nanodot. Due to the reduction of the effective field from the center to the edge, the frequency of edge mode is lower than that of CM.[16] For example, the CM is observed in nanodots with a diameter above 200 nm.[17,18] For smaller nanodots with a diameter below 200 nm, the inhomogeneous field near the edge dominates and the EM is observed in addition to the CM and leads to the enhancement of spin-wave spectra for laterally confined nanodots.[19,20] Moreover, the edge mode spectra are affected by the shape[21,22] and shape distortion[23–25] of nanodot.

Apart from the single layer nanodots, multilayer circular nanodots are found to show rich spin dynamic spectra due to the effects of long-range dipolar interactions or short-range exchange interactions. Moreover, dynamic magnetizations in two layers precess in-phase (known as an acoustic mode) and out-of-phase (known as an optical mode). This is analogous with the lattice dynamics, where acoustic mode (AM) corresponds to the in-phase atomic displacement and optical mode (OM) corresponds to the out-of-phase atomic displacement. Such in-phase and out-of-phase modes are found in multilayer thin films[26,27] and nanodots with various shapes.[28–31] The complex spin wave spectra of multilayered structures can be tuned by changing the thickness of non-magnetic metal spacer[32] or top layer in symmetric and asymmetric multilayer with the same material.[33] The effect of exchange coupling on spin wave spectra is observed in bilayer or trilayer stack of ferromagnet/non-magnet/ferromagnet (FM/NM/FM) with NM spacing less than the exchange length of FM metal. Above a certain thickness of the NM, the long range dynamic dipolar coupling plays a crucial role in changing the spin wave spectra.[34] For the circular trilayer nanodots, the formation of vortices, c-states, s-states or single domain, depends on the competition between magnetostatic coupling and exchange interactions in adjacent layers.[35,36] Further, with the application of an in-plane magnetic field, the uniform AM and OM are excited at saturation fields.

In the case of laterally confined layered structures, the acoustic and optical edge modes are observed in addition to CM.[37–39]

The previous works were limited to the investigation of the remanent states and dynamic behavior in thickness dependent laterally confined nanodots with an aspect ratio smaller than 0.1. Here, we have demonstrated how the effective field in the high aspect ratio (0.33 – 0.83) Py nanodots with different thicknesses changes the magnetization reversal and dynamic properties and compared these results with that of asymmetric trilayer nanodots. We have performed a comparative study on magnetization reversal mechanisms and microwave responses. A detailed micromagnetic simulation study has been carried out to unravel the origin of the FMR modes and magnetization reversal processes. We have analyzed that the magnetization reversal mechanism associated with vortex nucleation and annihilation fields and FMR mode frequencies are strongly sensitive to the thickness of the nanodot. Furthermore, we have shown the static and dynamic properties of trilayer nanodots by placing NM metal in between the thick and thin layers of Py. The magnetization reversal mechanism involves vortex nucleation in the thick layer. The optical center mode (OCM), acoustic center mode (ACM) and acoustic edge mode (AEM) are observed in laterally confined layered structures.

Methods

Arrays of circular Py ($Ni_{80}Fe_{20}$) single layer and trilayer nanodots (diameter d = 120) are fabricated over a large area of 5 × 5 mm^2 in a 240 nm thick resist film on top of a 60 nm thick bottom antireflection coating on silicon substrates at an exposure wavelength of 193 nm using deep ultraviolet (DUV) lithography technique. Single layer thicknesses (L) are 20 and 50 nm. The trilayer structure consists of two magnetic layers separated by a non-magnetic Palladium layer: Py(50 nm)/Pd(10 nm)/Py(20 nm). The details of the fabrication technique are described

elsewhere.[40] The fabrication process is followed by the electron beam deposition of Py films of various thicknesses, on top of a Cr (5 nm) adhesive layer, in a chamber, with a base pressure less than 5×10^{-8} Torr and the deposition rate is maintained at 0.2 Å/s. Thereafter, the samples are soaked in a DUV resist removal solution (0K 73 resist thinner) followed by lift-off in an ultrasonic bath.

A field emission scanning electron microscope (FESEM) is used to verify the lateral dimensions of the samples and to assess the quality of the fabrication. The dynamic properties in nanodots are detected using room temperature broadband FMR set up. The sample is placed on G-S-G (ground-signal-ground) type coplanar waveguide (CPW) in a flip-chip configuration. The signal of the CPW generates an excitation field h_{rf}, which is set to be perpendicular to the applied field H_{app} to have maximum excitation efficiency. The FMR spectra are extracted for excitation frequencies of h_{rf} from 5 to 16 GHz with a step of 0.5 GHz by sweeping the magnetic field from -300 mT to +300 mT with a step of 0.2 mT. The derivative of absorption response as a function of H_{app} is measured by a lock-in based technique where the H_{app} is modulated at a low frequency (490 Hz) using a Helmholtz coil and the data are recorded at the same reference frequency.

Micromagnetic simulations are performed using Object Oriented Micromagnetic Framework – OOMMF for the comprehensive understanding of magnetization reversal and dynamic behavior of the nanodots.[41] Standard parameters of Py are used in the simulations: saturation magnetization (Ms) = 8×10^{5} A/m, exchange constant (A) = 13×10^{-12} J/m, damping constant (α) = 0.008, magnetocrystalline anisotropy (K) = 0 and cuboidal cells of size 5 nm×5 nm×5 nm. It must be noted that the cell size (= 5 nm) is smaller than the exchange length defined by $l_{ex} = \sqrt{\frac{2A}{M_s{}^2\mu_0}}$ of Py (5.7 nm). The dimensions of the nanodot are determined from the FESEM images. To obtain the quasi-static magnetic configurations and magnetization reversals, we have

assumed a higher value of α = 0.5 for quick convergence – a standard practice in micromagnetic simulations without any significant deviations in the results. We have used a field step of 2 mT to obtain the hysteresis loop. To simulate FMR modes, a *sinc* pulse defined as $h_{rf} = h_0 \frac{\sin(2\pi f_c \tau)}{2\pi f_c \tau}$, where the amplitude of *sinc* wave h_0 = 5 mT, cut-off frequency f_c = 19 GHz and $\tau = t - t_0$ refers to the simulation time (t) with an offset t_0, is applied perpendicular to the bias field to maximize the torque (M×H).[42] We have performed a dynamic simulation for 4 ns with a step time of 10 ps. The dynamic magnetization data are post-processed in the frequency domain using the Fast Fourier Transform (FFT) procedure. We have analyzed magnetization as a function of position and time i.e. $M = M(x, y, z, t)$ to obtain the spatial FMR mode profiles.

Results and Discussion

Shown in Fig. 1(a) is the FESEM image of 50-nm-thick and 120-nm-diameter single layer nanodots with dot-to-dot separation s = 260 nm. In the case of our samples, the ratio $2s/d$ is 4.3 which is large and therefore the magnetostatic interaction between the dots can be ignored.[43] A schematic diagram of broadband FMR setup and zoom-in view of the G-S-G CPW on which an array of nanodots is placed in flip-chip configuration is shown in Fig. 1(b).

We begin by first simulating the hysteresis loops of single layer nanodots and trilayer nanodots as shown in Fig. 1(c). The hysteresis loops of single layer Py nanodots (L = 20 nm and 50 nm) consist of two triangular lobes with almost zero coercive field.[11] It suggests the presence of the vortex at the center in the ground state. The magnetization reversal process of nanodots involves nucleation, displacement and annihilation of the vortex. The switching fields at which the saturation state transforms to the vortex state and vice versa are known as vortex nucleation field (H_n) and annihilation field (H_a) respectively. To study the magnetization reversal mechanism, we

saturated the magnetization of the nanodot with H_{app} = +500 mT (> H_n) and swept the magnetic field over the field range ±200 mT. At high magnetic fields (> H_n), the magnetization is aligned in the direction of H_{app}. With the decrease in the field below H_n, there is an abrupt decrease in the magnetization parallel to the H_{app} and is characterized by the formation of the closure domain in the vortex state. This irreversible transition from the saturation to the vortex state is due to the competition among magnetostatic energy, exchange energy and Zeeman energy. The vortex starts to nucleate from the boundary of the nanodot. On decreasing the field, the vortex displaces towards the center of the nanodot by minimizing the magnetostatic energy and it reaches the center of the nanodot at zero field. There is a linear dependence of magnetization over a field range of $H_a < H_{app} < H_n$ and is the reversible part in the loop. On further decreasing the field along the $-x$ direction, the vortex destabilizes and annihilates at H_a which is accompanied by the sharp jump in the magnetization. Further, the magnetization gets saturated at negative high fields. The Magnetic configurations at different field positions of the hysteresis loops are shown in the inset of Fig. 1(c). The values of the H_n and H_a increase significantly with an increase in the thickness of the nanodot. For example, these critical field values are $\mu_0(H_n, H_a)$ = (0, −80) mT for the 20-nm-thick dots and (70, −120) mT for the 50-nm-thick dots.

Next, we focus on the magnetization reversal mechanism in asymmetric trilayer nanodot, Py(50)/Pd(10)/Py(20). The competition between interlayer dipolar energy and Zeeman energy are responsible for obtaining the stable magnetization configuration. The magnetic states near the switching fields of the trilayer are shown in the inset of Fig. 1(c). As the field is decreased down to 130 mT, the top Py layer starts to rotate its magnetization in opposite direction to the external field and the bottom Py layer aligns in the direction of the magnetic field. Both layers reach almost anti-parallel alignment near 50 mT, to minimize the stray field from the bottom layer. On further

decreasing the field from 50 mT, nucleation of the vortex in the thicker layer can be seen due to the dominance of exchange coupling over anti-ferromagnetic alignment between the layer through dipolar coupling. Vortex state is stable only in the bottom layer within the field range of 32 mT to −150 mT whereas there is no vortex state found in the top layer. The annihilation of the vortex state in the bottom layer takes place for the magnetic field beyond −150 mT.

To probe the magnetization dynamics in the structures described above, detailed field dependent FMR measurements were performed at ambient conditions. Figure 2(a) shows the measured FMR spectra for the single layer Py (L = 20 nm) nanodot array as a function of excitation frequency in the range from 6 GHz to 15 GHz. The resonance field (H_{res}) of the high intense peak increases with an increase in frequency. The values of the $\mu_0 H_{res}$ are 49, 109, 183 and 262 mT for 6, 9, 12 and 15 GHz, respectively. The zoom-in of the FMR spectrum is shown in the inset of the 9 GHz FMR spectrum to better visualize the low intense mode. Here, we observed a low intense peak with a large linewidth at the higher field of 183 mT. To get a better understanding of the results, we have performed dynamic micromagnetic simulations on a single nanodot by applying a field along x-axis and the *sinc* pulse along y-axis in order to mimic the experiments. We have plotted the simulated spectra in Fig. 2(b) at the experimental resonant fields as mentioned above. In agreement with our experimental results, we have found two modes in our simulations. To identify the origin of the modes we have analyzed 2D spatial profiles for power absorption and the images are attached in the inset of Fig. 2(b). The red and blue colours in the mode profile indicate the maximum and minimum power absorptions, respectively. The high intensity peak (labeled by 'star' symbol) is attributed as the CM (or uniform FMR) as mode profile clearly depicts the power absorption at the center of each nanodot. The low intense peak (labeled by ●-symbol) corresponds to the EM and mode profile shows the power absorption near the edges due to the inhomogeneous

effective magnetic field near the edges of the nanodot. The frequency of EM is less than that of CM in the 20-nm-thick dot. On comparing Fig 2 (a and b), we see a close match of the simulated star-mode which appears at 6.3, 8.8, 11.6 and 14.1 GHz with the most intense absorptions in the experimental FMR data. Hence, the most significant FMR modes are attributed to the CM. The EM is insignificant in our experiments with very weak intensity in comparison to the CM. We have shown the EM at 9 GHz by magnifying the data in Fig. 2(a). However, simulated spectra have considerably large EM intensity. We would like to point here that the simulations are conducted on an ideal nanodot. One of the ways to eliminate this difference between simulation and experiment is to use the SEM image as a mask for the simulation studies as shown in Fig. S1 in the supplementary material. Nevertheless, our assumption of using an ideal nanodot structure reflects the experimental trends correctly with significantly less computational time.

Figure 3 shows experimental and simulated results of H_{res} versus frequency with field variation from +300 mT to −300 mT for the 20-nm-thick dots. We can observe two different regions: the presence of CM and EM modes in the high field region and the absence of any FMR responses in a low field window near zero field. This low field window is found to be consistent with the simulated field window ($H_a < H_{app} < H_n$), where the presence of multiple peaks suggests a vortex state. For further insights, we have analyzed FMR spectra near the vortex formation region as shown in Fig. S2 in the supplementary material. Note that the frequencies of the vortex gyrations appear below 2 GHz which is the lower limit of our experimental set-up. Hence, the absence of the modes in FMR at the lower fields is most likely due to the vortex formations in the nanodots. On the other hand, CM and EM are found in the high field region (*i.e.* $H_{app} > H_n$ or $H_{app} < H_a$) and the frequency of these modes increases with increasing field. The FMR response with the variation of H_{app} is well understood from Kittel's formula[44],

$$f = \frac{\gamma \mu_0}{2\pi} \sqrt{\left[H_{app} + (N_z - N_x).M_s\right]\left[H_{app} + \left(N_y - N_x\right).M_s\right]}$$

Where $\frac{\gamma}{2\pi}$ = 28 GHz/T, μ_0 is magnetic permeability, N_x, N_y and N_z denote the demagnetizing factors in x-, y- and z- directions. Here the constraint equations are $N_x = N_y$ (circular dot) and $N_x+N_y+N_z = 1$. The H_{app} vs frequency was fitted with Kittel's formula. The trend of increase in the frequency with an increase in the resonance field (H_{res}) is supported using Kittel's formula. The fitted demagnetizing factors are $N_x = N_y = 0.05$ and $N_z = 0.886$. The results obtained from simulations for the CM and EM are within reasonable agreement and a slight mismatch can be attributed to the deviation of the nanodot shapes due to unavoidable lithographic irregularities within a large array of 5mm^2.

Next, we have investigated the thickness dependence and the effect of magnetostatic coupling on the resonant modes. Figure 4(a) shows the experimental FMR spectra for 20-nm-thick, 50-nm-thick and Py(50)/Pd(10)/Py(20) nanodots at a fixed excitation frequency of 10 GHz. We have observed two peaks at 130 mT (most intense) and 220 mT (low intense) for the 20-nm-thick nanodot. One high intense peak at 210 mT is found for the 50-nm-thick nanodot whereas any low intense mode is hardly distinguishable from the noise level and it could be due to the edge roughness which has smeared the EM contributions. Based on the micromagnetic simulations, the high intensity peak is attributed as CM (or uniform FMR) and the low intense peak corresponds to the EM and the results are also consistent with simulated spectra and 2D spatial profiles as shown in Fig. S3 in the supplementary material. The demagnetizing factors are obtained from fitting Kittel's formula for a clear understanding of H_{res} behaviour with an increase in the thickness. The demagnetizing factors are found to be $N_x = N_y = 0.213$ and $N_z = 0.57$. It can be seen that the H_{res}

increases with the increase in the thickness at a constant frequency. This is due to the change in the demagnetizing field with an increase in thickness.

For the trilayer nanodot, the ferromagnetic layers separated by Pd, we observed two well-resolved FMR peaks with different intensities. The low and high intense peaks lie at 200 and 250 mT respectively at the excitation frequency of 10 GHz. It is to be noted that the AM and OM are expected when multilayer nanodots are excited by h_{rf}. The AM are excited with symmetric excitation i.e, h_{rf} perpendicular to H_{app} and OM are excited with anti-symmetric excitation i.e., h_{rf} parallel to $H_{app.}$ In our measurement, we apply a uniform excitation field generated by the signal line which is perpendicular to H_{app} to probe the dynamics. As the uniform excitation field efficiently excites the AM, we can detect the high intense mode as AM. Nevertheless, our highly sensitive lock-in-based FMR tool still picks up weak OM (shown in the inset of Fig. 4 (a)). To understand the experimental data, we performed dynamic micromagnetic simulations and obtained 2D spatial profiles as shown in Fig. S4 in the supplementary material. In the low field region, the presence of multiple peaks suggests the presence of the vortex. Note that the separation (10 nm) between the top and bottom Py layers is greater than the exchange length (5.7 nm) of Py. Hence, the magnetic layers are only coupled through magnetostatic interactions in the trilayer nanodots. As we applied a uniform sinc pulse to excite the sample, we could detect only the AM.[37] Hence, at 250 mT, we obtained AM at 10 GHz which is in good match with experimental FMR spectra. In addition to AM and OM, we have noticed a low intense peak appearing at the low field. This peak is arising due to the inhomogeneous magnetization states near the low field region as shown in Fig. S5 in the supplementary material. This mode doesn't follow Kittel's Equation. The details are explained in the supplementary material.

To explore the field hysteresis of the dynamic responses, we have carried out FMR measurements by varying both the applied field (+300 mT to −300 mT) and excitation frequency (2-14 GHz). Figure 4(b) shows simulated and experimental results for 50-nm-thick nanodot. Note that EM mode is not observed in the whole range of the experimental FMR spectra which could be due to the edge roughness expected in a lithographic process for thicker dots. However, the experimental CM frequencies match well with the simulated spectra. The frequency of CM and EM increases with an increase in the applied field. Comparing the results of 20-nm-thick and 50-nm-thick dots, we can conclude that with the increase in the thickness, the resonance modes shift to the lower frequencies. A frequency variation of 4 GHz is found with the variation of thickness from 20 nm to 50 nm at 300 mT. This shift is due to the increase of demagnetizing field (decrease in the effective field) with an increase in thickness.

Figure 4(c) shows the experimental and simulated results for Py(50)/Pd(10)/Py(20) nanodot. As discussed above, we have found two center-type modes: an intense AM and a weak OM while varying the field for the tri-layer nanodot. The AM and OM correspond to the in-phase and out-of-phase precession of magnetization, respectively. The out-of-phase precession of magnetization increases the dynamic dipolar field of the system and enhances the effective field. Hence from the Kittel's equation, we can understand that the frequency of OM is greater than that of AM.[26] Hence the upper branch corresponds to the OM and the lower branch corresponds to the AM. The experimentally revealed modes can be well understood by performing the simulation. Uniform sinc pulse is used in the simulation and it could efficiently pick the AM. A good match between experimental and simulation AM is observed. The less intense mode in the simulation can be attributed to the acoustic edge mode.

Conclusions

To summarize, we have investigated the magnetization reversal and spin dynamics of single layer and asymmetric trilayer array of Py nanodots with a relatively high aspect ratio using the FMR technique. We found that the effective field and FMR mode profile markedly dependent on the thickness. The dynamic behavior displays two distinct modes, CM at high frequency and EM at low frequency. CM is the fundamental FMR mode that arises due to the excitation at the center of the nanodot. The inhomogeneity in the effective field near edges increases with a decrease in the thickness and gives rise to EM in addition to the CM. A significant increase in H_n and H_a and a notable decrease in the CM and EM frequency with an increase in the thickness are noticed in single layer nanodots. For trilayer nanodot, the existence of AM and OM is noticed due to the dipolar coupling between the adjacent ferromagnetic layers separated by 10-nm Pd. Our experimental results are consistent with micromagnetic simulation results. These results can be useful for nanoscale magnonic applications.

Supplementary Material

See supplementary material for the plots of edge roughness dependent, field-dependent simulated spin dynamics for all the samples and analysis of low intensity modes in the trilayer.

Data Availability Statement

The data that supports the findings of this study are available within the article and its supplementary material.

Acknowledgments

A.H. would like to thank the funding under the Ramanujan Fellowship (SB/S2/RJN-118/2016), Department of Science and Technology (DST), India. AOA would like to acknowledge the funding from the Royal Society and Wolfson Foundation. Dr. Navab Singh is thanked for the DUV templates.

References

[1] R.P. Cowburn and M.E. Welland, Science (80-.). **287**, 1466 (2000).

[2] A. Imre, G. Csaba, L. Ji, A. Orlov, G.H. Bernstein, and W. Porod, Science (80-.). **311**, 205 (2006).

[3] Y. Shiroishi, K. Fukuda, I. Tagawa, H. Iwasaki, S. Takenoiri, H. Tanaka, H. Mutoh, and N. Yoshikawa, IEEE Trans. Magn. **45**, 3816 (2009).

[4] S.I. Klselev, J.C. Sankey, I.N. Krivorotov, N.C. Emley, R.J. Schoelkopf, R.A. Buhrman, and D.C. Ralph, Nature **425**, 380 (2003).

[5] G. Csaba, A. Imre, G.H. Bernstein, W. Porod, and V. Metlushko, IEEE Trans. Nanotechnol. **1**, 209 (2002).

[6] B. Van Waeyenberge, A. Puzic, H. Stoll, K.W. Chou, T. Tyliszczak, R. Hertel, M. Fähnle, H. Brückl, K. Rott, G. Reiss, I. Neudecker, D. Weiss, C.H. Back, and G. Schütz, Nature **444**, 461 (2006).

[7] D. Kumar, S. Barman, and A. Barman, Sci. Rep. **4**, 4108 (2014).

[8] M. Tarequzzaman, T. Böhnert, M. Decker, J.D. Costa, J. Borme, B. Lacoste, E. Paz, A.S. Jenkins, S. Serrano-Guisan, C.H. Back, R. Ferreira, and P.P. Freitas, Commun. Phys. **2**, 1 (2019).

[9] R.P. Cowburn, J. Magn. Magn. Mater. **242**–**245**, 505 (2002).

[10] R.P. Cowburn, D.K. Koltsov, A.O. Adeyeye, M.E. Welland, and D.M. Tricker, Phys. Rev. Lett. **83**, 1042 (1999).

[11] K.Y. Guslienko, J. Nanosci. Nanotechnol. **8**, 2745 (2008).

[12] J. Ding, G.N. Kakazei, X. Liu, K.Y. Guslienko, and A.O. Adeyeye, Sci. Rep. **4**, 4796 (2014).

[13] D. Kumar, P. Lupo, A. Haldar, and A.O. Adeyeye, Appl. Phys. Lett. **108**, 192404 (2016).

[14] R.V. Verba, A. Hierro-Rodriguez, D. Navas, J. Ding, X.M. Liu, A.O. Adeyeye, K.Y. Guslienko, and G.N. Kakazei, Phys. Rev. B - Condens. Matter Mater. Phys. **93**, 214437 (2016).

[15] F.G. Aliev, J.F. Sierra, A.A. Awad, G.N. Kakazei, D.S. Han, S.K. Kim, V. Metlushko, B. Ilic, and K.Y. Guslienko, Phys. Rev. B - Condens. Matter Mater. Phys. **79**, 174433 (2009).

[16] G. Carlotti, Appl. Phys. Rev. **6**, 031304 (2019).

[17] J.F. Sierra, A.A. Awad, G.N. Kakazei, F.J. Palomares, and F.G. Aliev, IEEE Trans. Magn. **44**, 3063 (2008).

[18] G. Shimon and A.O. Adeyeye, Appl. Phys. Lett. **109**, 032407 (2016).

[19] X.K. Hu, H. Dey, N. Liebing, H.W. Schumacher, G. Csaba, A. Orlov, G.H. Bernstein, and W. Porod, J. Appl. Phys. **117**, 243905 (2015).

[20] F. Guo, L.M. Belova, and R.D. McMichael, Phys. Rev. Lett. **110**, 1 (2013).

[21] B. Rana, D. Kumar, S. Barman, S. Pal, Y. Fukuma, Y. Otani, and A. Barman, ACS Nano **5**, 9559 (2011).

[22] G. Carlotti, S. Tacchi, G. Gubbiotti, M. Madami, H. Dey, G. Csaba, and W. Porod, J. Appl. Phys. **117**, 17A316 (2015).

[23] J.M. Shaw, T.J. Silva, M.L. Schneider, and R.D. McMichael, Phys. Rev. B - Condens. Matter Mater. Phys. **79**, 184404 (2009).

[24] P.S. Keatley, P. Gangmei, M. Dvornik, R.J. Hicken, J. Grollier, and C. Ulysse, Phys. Rev.

Lett. **110**, 187202 (2013).

[25] H.T. Nembach, J.M. Shaw, T.J. Silva, W.L. Johnson, S.A. Kim, R.D. McMichael, and P. Kabos, Phys. Rev. B - Condens. Matter Mater. Phys. **83**, 094427 (2011).

[26] Y. Song, D. Cao, H. Du, M. Liu, S. Du, C. Song, Q. Li, J. Xu, and S. Li, J. Appl. Phys. **126**, 213902 (2019).

[27] J. Robinson, K. Xi, R.V. Kumar, A.C. Ferrari, H. Au, M.-M. Titirici, A. Parra Puerto, A. Kucernak, S.D.S. Fitch, and N. Garcia-Araez, J. Phys. Energy **2**, 0 (2017).

[28] V. V. Naletov, G. De Loubens, G. Albuquerque, S. Borlenghi, V. Cros, G. Faini, J. Grollier, H. Hurdequint, N. Locatelli, B. Pigeau, A.N. Slavin, V.S. Tiberkevich, C. Ulysse, T. Valet, and O. Klein, Phys. Rev. B - Condens. Matter Mater. Phys. **84**, 224423 (2011).

[29] F. Montoncello, L. Giovannini, and F. Nizzoli, J. Appl. Phys. **105**, 07E304 (2009).

[30] M. Madami, G. Carlotti, G. Gubbiotti, F. Scarponi, S. Tacchi, and T. Ono, J. Appl. Phys. **109**, 07B901 (2011).

[31] G. Gubbiotti, M. Madami, S. Tacchi, G. Carlotti, H. Tanigawa, and T. Ono, J. Phys. D. Appl. Phys. **41**, 134023 (2008).

[32] X. Zhou and A.O. Adeyeye, Phys. Rev. B **94**, 054410 (2016).

[33] G. Gubbiotti, S. Tacchi, H.T. Nguyen, M. Madami, G. Carlotti, K. Nakano, T. Ono, and M.G. Cottam, Phys. Rev. B - Condens. Matter Mater. Phys. **87**, 094406 (2013).

[34] A.A. Awad, A. Lara, V. Metlushko, K.Y. Guslienko, and F.G. Aliev, Appl. Phys. Lett. **100**, 262406 (2012).

[35] Z. Yan, X. Fan, and Z. Li, Nanoscale Res. Lett. **9**, 106 (2014).

[36] K.S. Buchanan, K.Y. Guslienko, A. Doran, A. Scholl, S.D. Bader, and V. Novosad, Phys. Rev. B - Condens. Matter Mater. Phys. **72**, 134415 (2005).

[37] M. Dvornik, P. V. Bondarenko, B.A. Ivanov, and V. V. Kruglyak, J. Appl. Phys. **109**, 07B912 (2011).

[38] Z. Zeng, K.H. Cheung, H.W. Jiang, I.N. Krivorotov, J.A. Katine, V. Tiberkevich, and A. Slavin, Phys. Rev. B - Condens. Matter Mater. Phys. **82**, 100410 (2010).

[39] G. Gubbiotti, M. Madami, S. Tacchi, G. Carlotti, and T. Okuno, Phys. Rev. B - Condens. Matter Mater. Phys. **73**, 144430 (2006).

[40] A.O. Adeyeye and N. Singh, J. Phys. D. Appl. Phys. **41**, 153001 (2008).

[41] M.J.D. and D.G. Porter, Interag. Rep. NISTIR 6376, Natl. Inst. Stand. Technol. Gaithersburg, MD (Sept 1999) (n.d.).

[42] D. Kumar, O. Dmytriiev, S. Ponraj, and A. Barman, J. Phys. D. Appl. Phys. **45**, 015001 (2012).

[43] K.Y. Guslienko, Appl. Phys. Lett. **75**, 394 (1999).

[44] C. Kittel, Phys. Rev. **73**, 155 (1948).

List of figures:

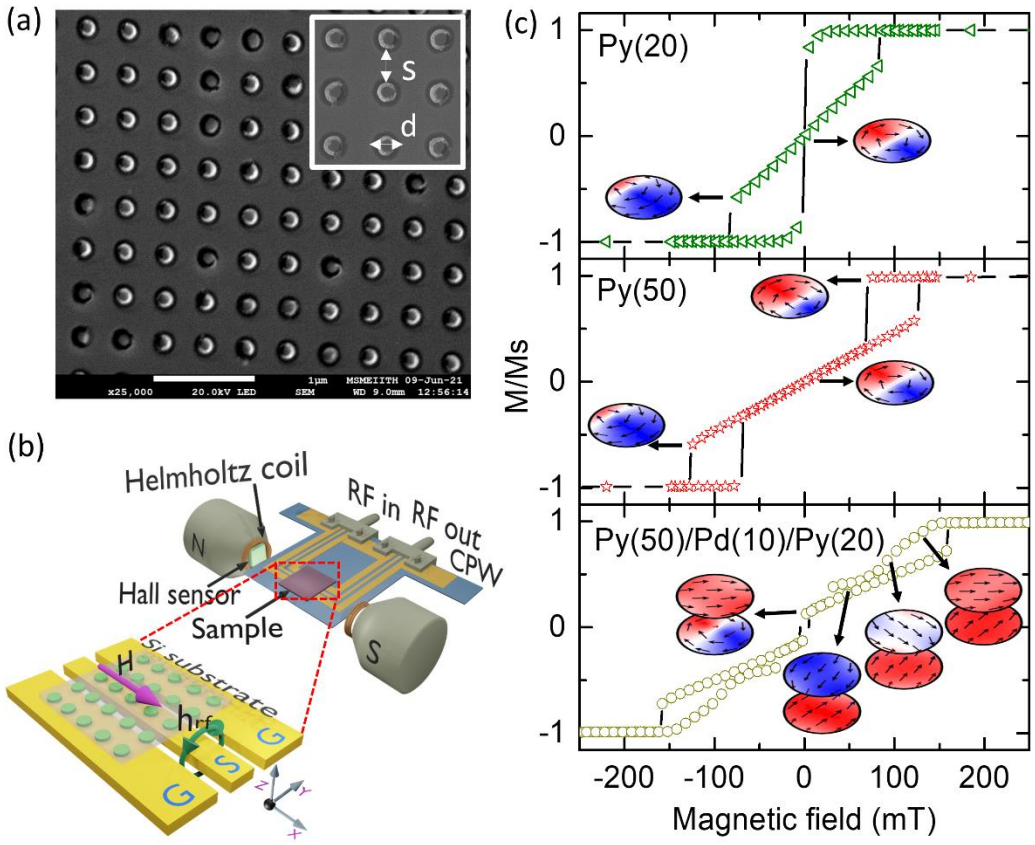

Figure 1: (a) FESEM image of 50-nm-thick Py nanodot describing the lateral dimensions s = 260 nm and d = 120 nm in the inset. (b) Schematic diagram of FMR experiment setup. (c) Simulated hysteresis loops for single layer nanodot array with thicknesses 20 nm and 50 nm. and trilayer nanodot Py(50)/Pd(10)/Py(20). The remanent states are shown in the inset.

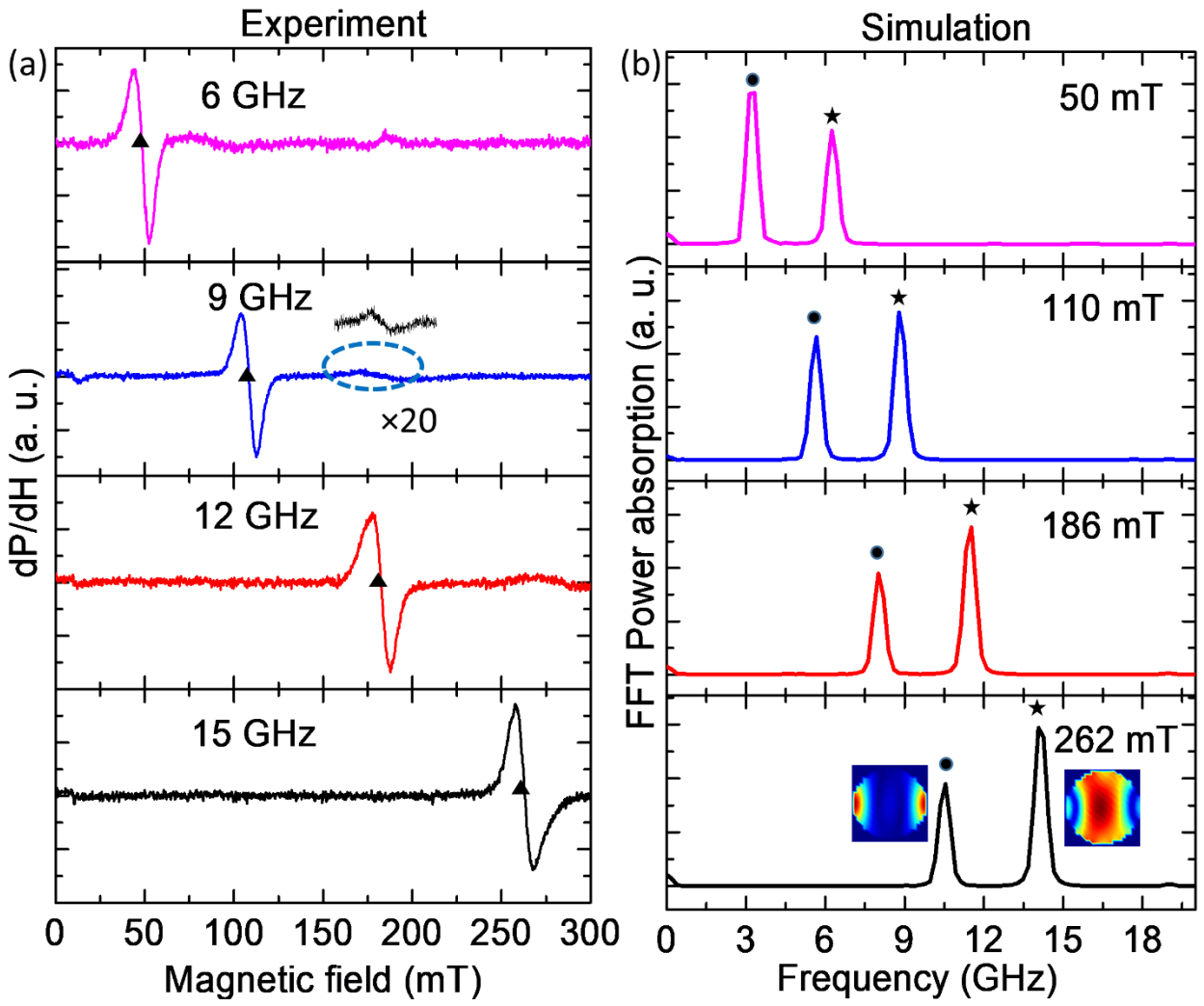

Figure 2: (a) Experimental FMR Spectra at 6 GHz, 9 GHz, 12 GHz and 15 GHz and (b) simulated FMR Spectra at 50 mT, 110 mT, 186 mT and 262 mT of the 20-nm-thick dot. Round and star symbols denote the edge and center modes, respectively. The red and blue color indicates maximum and minimum power absorption. Triangular dots in Fig. 2(a) indicate the position of the H_{res}.

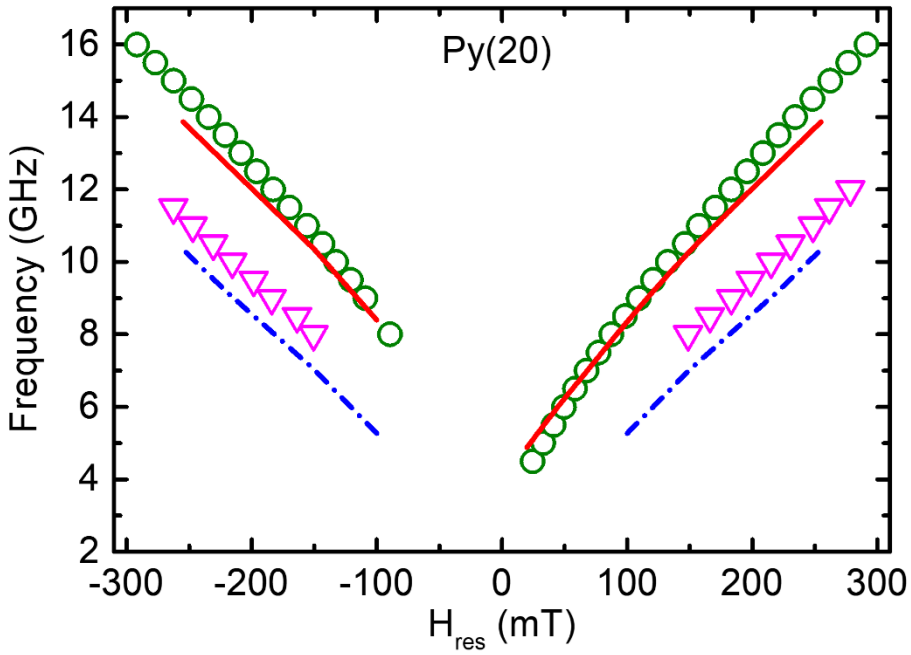

Figure 3: Frequency of center and edge modes versus H_{res} plot for 20-nm-thick dot.. Open circle and open down triangle are experimental center and edge mode spectra respectively. Solid line and dash-dot-line are simulation data for center and edge mode spectra, respectively.

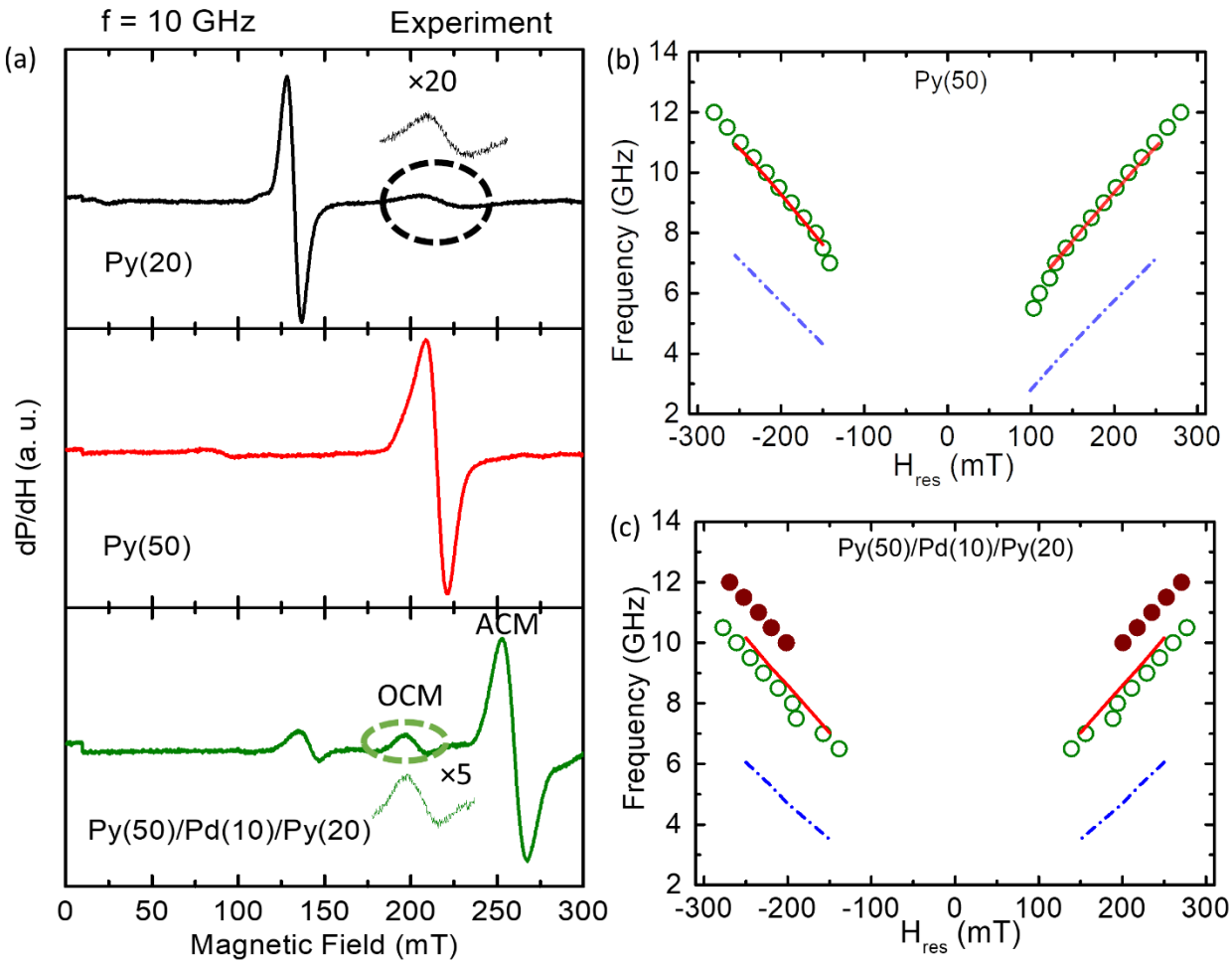

Figure 4: (a) Experimental FMR spectra of single and trilayer nanodot arrays. Frequency of center and edge modes versus H_{res} plot for (b) 50-nm-thick nanodot and (c) trilayer nanodot array. Open and close circular symbols represent experimental data for acoustic and optical center mode spectra, respectively. Solid line and dash-dot-line correspond to simulation data for center and edge mode spectra, respectively.